Journal of Materials Chemistry

Cite this: *J. Mater. Chem.*, 2012, **22**, 7837

www.rsc.org/materials

PAPER

Controlling vertical alignment of phthalocyanine nanofibers on transparent graphene-coated ITO electrodes for organic field emitters†

Kuo-Jung Huang,[a] Yu-Sheng Hsiao,*[b] Jen-Hsien Huang,[b] Chih-Wei Chu,[b] Peilin Chen[b] and Wha-Tzong Whang*[a]

Received 19th January 2012, Accepted 22nd February 2012
DOI: 10.1039/c2jm30383c

In this study, we developed a simple and efficient approach—using graphene coatings on ITO as transparent electrodes—for inducing the growth of 29*H*,31*H*-phthalocyanine (H_2Pc) nanofiber arrays through a thermal evaporation process, with potential use in organic field emitters (FEs). By controlling the surface energy and temperature of the electrodes during evaporation, H_2Pc molecules readily self-assemble, forming an out-of-plane morphology on reduced graphene oxide surfaces (rGO; surface energy: *ca.* 50 mJ m^{-2}). The devices fabricated on rGO/indium tin oxide (**FE-rGO**) exhibited not only excellent FE performance but also outstanding anti-degradation capability during stability tests. This facile approach toward rGO coatings opens a new avenue for the transformation of small organic molecule films into vertically standing nanostructures on transparent electrodes, with various organic electronics applications.

1. Introduction

Graphene sheets, carbon materials consisting of single-atom-thick sp^2-hybridized carbon atoms, have high specific surface areas and high conductivity.[1,2] Due to their exceptional opto-electronic properties, including electrical conductivity,[2] optically transparency,[3] mechanical flexibility,[3,4] and chemical/thermal stability,[5–7] graphene films have become promising electrode candidates to replace precious metal/metal oxides in future flexible electronics and optoelectronics. Graphene was first isolated from bulk graphite using exfoliation techniques.[1] At present, several effective approaches are available for the preparation of graphene in high yields.[8–10] The large-scale production of single-layer graphene through chemical exfoliation is most commonly used because of its convenience, high efficiency, and feasibility. It involves chemical oxidation of graphite to hydrophilic graphite oxide—using the so-called "Hummers method"[11]—with subsequent exfoliation into individual graphene oxide (GO) sheets through ultrasonication[9] and oxidative aqueous dispersion; the GO is subsequently converted back to conducting graphene (rGO) through chemical reduction, transforming the sheets from electrically insulating to conducting states. In addition to providing large quantities of graphene thin films exhibiting flexibility, electrical conductivity, and optical transparency, this facile solution process is also a straightforward approach toward fabricating patterned electrodes (*e.g.*, through ink-jet printing or stamp transferring)[12–15] for organic electronics.

One-dimensional (1D) organic nanostructures based on the π-stacking of small molecules have received growing attention because of their unique properties relative to those of their bulk counterparts. Compared with inorganic nanomaterials, 1D organic nanomaterials have several advantageous characteristics, including low cost, preparation through low-temperature processing, and mechanical flexibility. The self-assembly of phthalocyanine derivatives in particular has been used to prepare a variety of nanostructures for use in organic electronics [*e.g.*, the in-plane morphology for light emitting diodes[16] and field-effect transistors;[17–20] the out-of-plane morphology for solar cells[21–23] and field emission (FE) devices].[24–26] The growth mechanisms of organic thin films on substrates are complicated because of specific issues related to each type of organic molecule; for example, the effects of the surface energy of substrates, non-covalent interactions at the molecule/substrate interface, and intermolecular forces between molecules would result in different morphologies of small-molecule films.[26] Recently, a method was reported for fabricating 1D nanostructures of small-molecule films by tuning various growth conditions under vacuum conditions; this approach, which was mainly ascribed to Stranski–Krastanov growth on the supporting surfaces,[27] provided materials exhibiting outstanding electronic properties that enhanced device performance.[24–26,28–30] Notably, the surface

[a]*Department of Materials Science and Engineering, National Chiao Tung University, Hsinchu 30010, Taiwan, ROC. E-mail: wtwhang@mail.nctu.edu.tw; Fax: +886-35-724727; Tel: +886-35-731873*
[b]*Research Center for Applied Sciences, Academia Sinica, Taipei 11529, Taiwan, ROC. E-mail: yshsiao@gate.sinica.edu.tw; Fax: +886-2-27826680; Tel: +886-2-27898000-21*
† Electronic supplementary information (ESI) available. See DOI: 10.1039/c2jm30383c

energy and substrate temperature (T_{sub}) are two important factors affecting the morphologies of small-molecule films prepared through conventional thermal evaporation (TE).[23,25,26] The transition from in-plane to vertical morphology that occurred upon increasing the value of T_{sub} can be explained by considering the following equation:[31]

$$\gamma_s = \gamma^0[1 - (T_s/T_c)]^n \quad (1)$$

where γ_s is the surface energy at the substrate temperature T_s and γ^0 is the surface energy at the critical temperature (T_c); the value of n may be close to unity for cathodes. This formula suggests that the SE of the substrate (γ_s) decreases as the substrate temperature increases, thereby favoring desorption and surface diffusion of organic molecules. Especially for the noble metal surfaces[25,26] (*e.g.*, Au, Ag) appearing nonreactive to molecules, a decrease in surface energy weakens the molecule–substrate interactions, causing the molecule–molecule interactions (*i.e.*, π–π and van der Waals interactions) to become dominant. Therefore, a nanofiber structure of small-molecule films can be fabricated readily by increasing the value of T_{sub} to a certain level; such structures are presumed to be effective active layers for use in optoelectronic applications. Nevertheless, how to use transparent electrodes for inducing vertical alignment of small-molecule nanostructure films has not yet been fully investigated in optoelectronic devices.

In this study, we used an aqueous GO solution and subsequent chemical reduction to modify an indium tin oxide (ITO) electrode with an rGO coating to decrease the surface energy of the pristine substrate. Combining the manipulation of the surface energy and the value of T_{sub} through a TE process, we obtained H_2Pc nanofiber films on the highly uniform, large-area rGO surfaces for use in FE applications. We used scanning electron microscopy (SEM) and high-resolution transmission electron microscopy (HRTEM) to characterize the morphologies of these 1D H_2Pc nanofiber films, and X-ray photoelectron spectroscopy (XPS) and micro-Raman spectroscopy to characterize the defect density of the GO and rGO films. Furthermore, we used Raman mapping to monitor the uniformity of the rGO films on the ITO glass. To explore the competing potential for using rGO coatings on ITO as transparent electrodes in devices, we also prepared H_2Pc nanofiber films on opaque Ag surfaces as a reference for FE applications. To investigate the FE characteristics of these H_2Pc nanofiber films on rGO/ITO and Ag/ITO electrodes, we used a vacuum emission measurement (VEM) system to examine their FE properties; to study their practicability, we also performed stability tests using the two FE devices.

2. Experimental details

2.1 Preparation of samples

GO was prepared from natural graphite using a modified Hummers method.[11] A fully exfoliated GO aqueous dispersion was achieved after sonication for 2 h and subsequent centrifugation (2500 rpm) for 30 min. The resulting GO aqueous solution (0.1 wt%, 10 mg) was mixed with methanol (8 mL) and H_2O (2 mL) for spin casting. A GO film was spin-cast upon an ITO substrate [Fig. 1(A, B)]. Finally, the GO film was chemically reduced in hydrazine vapor at 110 °C for 6 h to obtain the large-scale reduced GO layers on ITO glass [Fig. 1(C)]. The Ag/ITO substrate was prepared by depositing Ag films (1000 Å) onto the ITO substrate [Fig. 1(D)]. For comparison of UV–Vis spectra of various carbon-coated and Ag-coated ITO electrodes, a 20Ag/ITO substrate was prepared by depositing an ultrathin (20 Å) layer of Ag onto ITO glass using an electron beam evaporator operated at a base pressure of 8×10^{-7} Torr. The corresponding deposition rates, controlled by a quartz crystal microbalance, were 0.2 Å s^{-1} for the 20Ag/ITO and 1 Å s^{-1} for the Ag/ITO substrate.

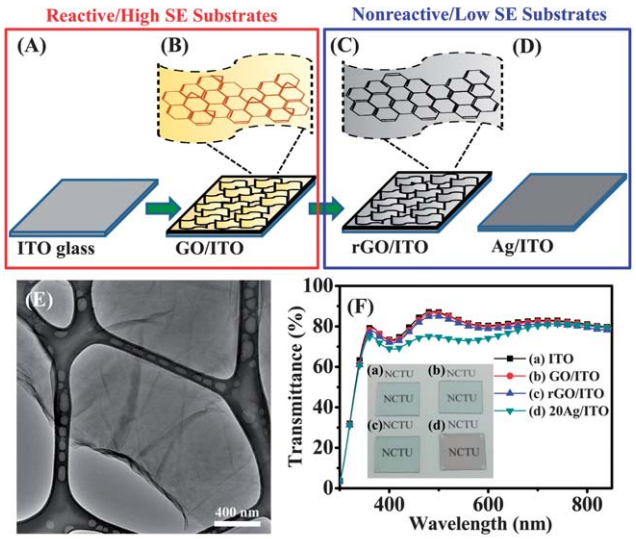

Fig. 1 (A–D) Schematic representation of the fabrication of various coatings of ITO substrates. (E) TEM image of a GO sheet, displaying a smooth and flat structure with a few folds. (F) UV–Vis spectra of ITO, GO/ITO, rGO/ITO and 20Ag/ITO [ultrathin (20 Å) Ag films on ITO glass] substrates. Inset: Optical images of substrates modified with carbon-based and ultrathin Ag films.

H_2Pc thin films were deposited using a thermal evaporator operated at a base pressure of 5×10^{-6} Torr. A commercially available H_2Pc powder (purity: 99%; Acros Industry) was used as received; it was sublimed onto four kinds of substrates (ITO, GO/ITO, rGO/ITO and Ag/ITO). The deposition time for the ITO, GO/ITO, and rGO/ITO substrates was 30 min; for the Ag/ITO substrates, it was 15 min. During the sublimation process, the value of T_{sub} for all substrates was maintained at 230 °C. The sublimation of the H_2Pc powder was performed at a crucible temperature of 150 °C; the corresponding deposition rate, controlled by a quartz crystal microbalance, was 0.5 Å s^{-1}.

Thin films of copper phthalocyanine (CuPc), coronene, and 1,5-diaminoanthraquinone (DAAQ) were deposited using a thermal evaporator operated at a base pressure of 5×10^{-6} Torr. Commercially available CuPc (purity: 99%; Acros Industry), coronene (purity: 95%; Acros Industry), and DAAQ (purity: 92%; Tokyo Chemical Industry) powder were used as received; they were sublimed individually onto rGO/ITO substrates. The deposition time for the CuPc films was 10 min; for the coronene and DAAQ films, it was 5 min. During the sublimation process, the value of T_{sub} was maintained at 230 °C for the CuPc films and at room temperature for the coronene and

DAAQ films. The sublimations of the CuPc, coronene, and DAAQ powders were performed at crucible temperatures of 170, 55, and 42 °C, respectively; the corresponding deposition rate, controlled by a quartz crystal microbalance, was 0.5 Å s^{-1}.

2.2 Characterization techniques

Top and cross-sectional views of the morphologies of the H_2Pc thin films were recorded using a JEOL JSM-6500F scanning electron microscope. An alcoholic dispersion of H_2Pc nanofibers was achieved by sonication for 10 min. The resulting nanofibers solution was subsequently dropped onto the TEM grid with a lacey carbon support film (Agar Sci., Inc.). The TEM, HRTEM images and the corresponding selected area electron diffraction (SAED) patterns of H_2Pc nanofibers were obtained using a JEOL-2010-F TEM at an accelerating voltage of 200 kV. Contact angles were determined on each substrate using the geometric mean approximation with two standard liquids: water (H_2O) and diiodomethane (CH_2I_2). The surface energies of the substrates were calculated using the Owens and Wendt method.[32] The structural phases of the GO and rGO films were characterized using micro-Raman spectroscopy (alpha 300, WITec Instruments Corp., Germany), with a resolution of 1 cm^{-1} and excitation with the 488 nm Ar-ion laser line. XPS spectra were recorded using a VG scientific Microlab 350 spectrometer operated in the constant analyzer energy mode with a pass energy of 40 eV, with Mg-Kα (1253.6 eV) radiation as the excitation source (with normal emission detected). The work function of the rGO substrate, and the valence band [highest occupied molecular orbital (HOMO)] of the H_2Pc materials were surveyed using photoelectron spectroscopy in air (PESA; AC–2 photoelectron spectrometer); the Riken Keiki apparatus detected the number of photo-emitted electrons per second (CPS) as a function of the photon energy, using a UV light source for excitation and a gas-flow Geiger counter. The relationship between CPS and the photon energy is described using the approximate equation[33]

$$\mathrm{CPS}^{1/2} = \frac{M}{k}(h\nu - \phi) \quad (2)$$

where M is an emission constant, k is the Boltzmann constant, $h\nu$ is the photon energy, and ϕ is the work function. When the surface materials were bombarded under a gradually increasing amount of UV light, photoelectrons were emitted from the surface (from a depth of several to a hundred angstroms) at a certain energy level, due to the photoelectron effect. These emitted photoelectrons were then counted by a detector and open counter. The value of ϕ was determined through linear extrapolation of $\mathrm{CPS}^{1/2}$ to zero yield,[33] when the PESA data were fitted using the software supplied with the spectrometer. UV–visible (UV–Vis) spectra (300–1100 nm) of H_2Pc thin films were recorded using a Shimadzu UV–3600 spectrophotometer.

The FE characteristics of the H_2Pc nanofibers were determined using a VEM system under a base pressure of 5×10^{-6} Torr. ITO plate glass was used as the anode, positioned above the cathode surface at a distance of 60 μm. The FE instrument featured a plate-to-plate geometry; the active area of the H_2Pc nanofiber arrays was 0.06 cm^2. Current density–electric field (J–E) curves of the FE devices were measured using the source monitor unit of a Keithley 237 instrument (accuracy: 10^{-13} A). The emission currents of the H_2Pc nanofibers were monitored as a function of the sweep bias. A dc voltage with a sweep step of 20 V was applied from 0 to 780 V to the sample to supply an electric field. Stability tests were performed for 3600 s under a constant applied field of 12 V μm^{-1} at room temperature.

3. Results and discussion

In this study, we explored the rGO coating as the surface modification layer to tailor the ITO surface from a reactive high surface energy (SE) surface to a nonreactive low SE surface. Therefore, we prepared ITO glass substrates presenting coatings of GO, reduced GO, and Ag (GO/ITO, rGO/ITO and Ag/ITO, respectively), with decreased SE from an initial value of 74.6 mJ m^{-2} to 66.2, 50.7, and 34.8 mJ m^{-2}, respectively (Table 1). A schematic representation of the fabrication of the various coatings on the ITO electrodes is shown in Fig. 1(A–D). Fig. 1(E) displays a TEM image of the GO sheets; the slightly wrinkled and folded paper-like structure reveals that exfoliated GO sheets had been prepared successfully using the Hummers method.[11] Furthermore, to explored the possibility of fabricating nanofiber films on transparent electrodes, we recorded the optical spectra of ITO, GO/ITO, rGO/ITO, and 20Ag/ITO [ultrathin (20 Å) Ag films on ITO glass] electrodes, obtaining transmissions of 82.3, 82.0, 80.9, and 73.0%, respectively, at a wavelength of 550 nm [Fig. 1(F)]. A photograph of the four different electrodes [Fig. 1(F), inset] confirms their high transparencies and reveals their suitability for use as transparent front electrodes.

As indicated in Fig. 2, different SEs of the electrodes resulted in different morphologies of H_2Pc thin films prepared through TE at a value of T_{sub} of 230 °C; the thickness of H_2Pc thin films grown in the first step is presented by the letter T, and the length and diameter of the rods grown in the second step[23] [Fig. 2(I, J)]. The high SE of ITO substrates featuring a strong chemical interaction between the H_2Pc/ITO interface would disorder the self-assembly behavior of H_2Pc molecules.[34] Therefore, the SEM image of entangled, tilted, and in-plane fiber-like morphologies of H_2Pc thin films on the ITO substrate revealed the thicker T (~200 nm) in the first step [Fig. 2(A, E)]. Similar to the reactive high SE of ITO substrates, the in-plane fiber-like morphology of the H_2Pc thin films on the GO/ITO substrate was also observed in Fig. 2(B, F). GO films have a wide range of oxygen-containing functionalities, such as 1,2-epoxide and alcohol groups on the basal planes, and carboxyl and ketone groups at the edges.[35,36] Therefore, the strong chemical interaction occurred at the H_2Pc/GO interface by the amide linkage.[37] During the sublimation process of H_2Pc molecules at the value of T_{sub} of 230 °C, this strong interaction between H_2Pc molecules and oxygen functional groups was believed to decrease the desorption and surface diffusion of H_2Pc molecules. Relative to the ITO surface, the GO/ITO surface significantly affects the stacking behavior of H_2Pc molecules, thereby inhibiting the growth of nanostructural morphologies of H_2Pc thin films on GO/ITO substrates. In contrast, we obtained high-quality vertical alignment of H_2Pc nanofiber films with thinner T on the nonreactive low SE of rGO/ITO and Ag/Si substrates [Fig. 2(C, G) and (D, H), respectively]. Most of the self-assembled H_2Pc nanofibers grew perpendicularly (with slight slanting) from the substrates to form

Table 1 Contact angles and surface energies of the various substrates

Substrate	Contact angle (°)		Surface energy[a] (mJ m^{-2})
	Water (H_2O)	Diiodomethane (CH_2I_2)	
ITO	23.9 ± 1.8	27.4 ± 0.9	74.6
GO/ITO	46.3 ± 1.3	36.1 ± 0.7	66.2
rGO/ITO	70.7 ± 2.7	34.2 ± 1.9	50.7
Ag/ITO	96.8 ± 1.4	51.9 ± 0.7	34.8

[a] Calculated using the Owens method from the geometric mean approximation (GMA) measurements of the static contact angles of H_2O and CH_2I_2.

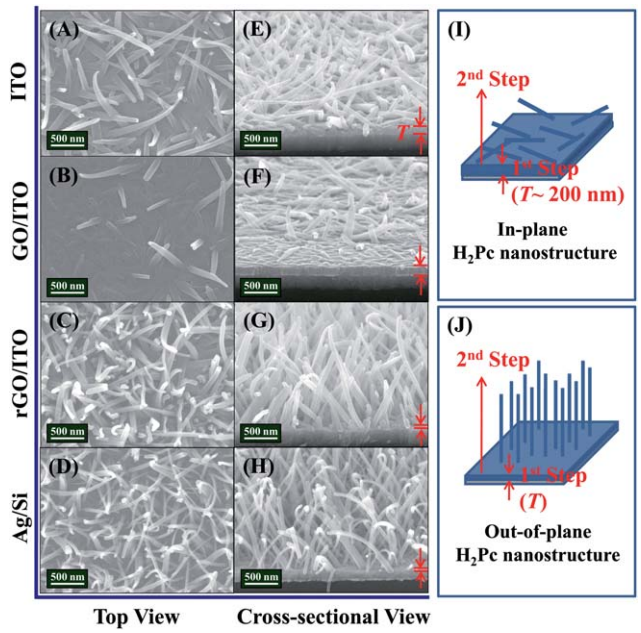

Fig. 2 Top-view and cross-sectional SEM images of H_2Pc thin films deposited on (A, E) ITO, (B, F) GO/ITO, (C, G) rGO/ITO and (D, H) Ag/Si substrates at a value of T_{sub} of 230 °C. (I, J) Schematic representations of in-plane and out-of-plane H_2Pc nanostructures.

quasi-arrays, presumably because repulsive forces among the nuclei would result in a parallel-displaced conformation.[30]

Raman spectroscopy is highly sensitive to the structure of graphitic materials, making it an essential tool for identifying differences in their electronic structures. In this study, we recorded the Raman spectra of GO and rGO [Fig. 3(A)] to characterize their degrees of reduction before and after performing the chemical reduction process. Graphitic structures typically display two features: a peak near 1595 cm^{-1} (G band), related to the vibration of sp^2-bonded carbon atoms in a two-dimensional hexagonal lattice, and a peak near 1340 cm^{-1} (D band), related to the defects and disorder in the hexagonal graphitic layers.[38–41] We calculated the ratio of the intensities of the D and G bands (I_D/I_G), generally accepted to reflect the density of defects and the degree of graphitization of graphitic materials,[38–40] to be 0.96 for GO and 1.15 for rGO prepared using the hydrazine reduction method. Thus, a slightly increase in the I_D/I_G ratio occurred after chemical reduction, suggesting a greater number of much smaller sp^2 domains upon reduction of the exfoliated GO.[42] The Raman mapping image (G band) revealed a large-area, uniform coating of overlapping rGO sheets on the ITO surface [Fig. 3(B)], presumably effectively decreasing the surface energy of ITO from 74.6 to 50.7 mJ m^{-2} and subsequently inducing the growth of the H_2Pc nanofiber films.

To verify the hydrazine reduction of GO into rGO, the C1s XPS spectra were recorded to understand the changes of graphene defects [Fig. 3(C, D)]. As shown in Fig. 3(C), two obvious peaks at binding energies of about 284.3 and 286.4 eV for GO represent the graphitic C=C (C–C) and oxygen-containing functionalities. The deconvolution of the C1s peak of GO further analyzed by nonlinear regression with models displays five peaks located at binding energies of 284.3, 285.4, 286.4, 288 and 289.1 eV, which can be assigned to the (1) C=C (C–C), (2) C–OH, (3) C–O–C (epoxide), (4) C=O (carbonyl C) and (5) O=C–OH (carboxylate C) functional groups, respectively. Therefore, the presence of these groups on the surface of GO essentially enabled GO to bear negative charges and have good water dispersibility. After the chemical reduction, the small amount of oxygen-containing functionalities were observed with fewer defects [Fig. 3(D)], thereby minimizing the SE and reactivity with organic molecules. In addition, the atomic percentages of carbon

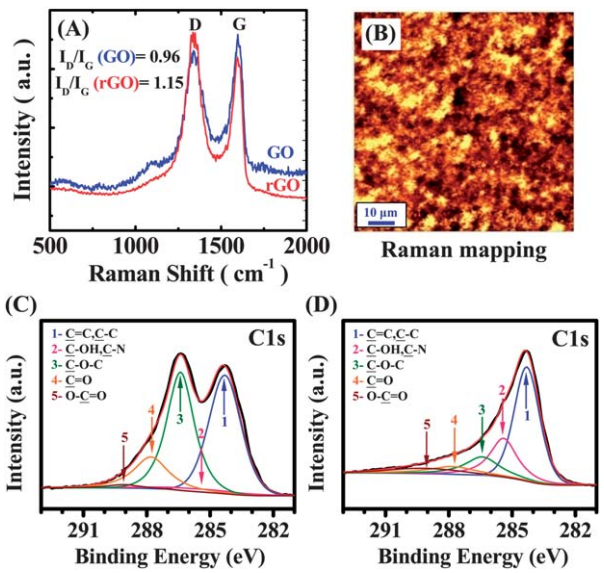

Fig. 3 (A) Raman spectra of GO and rGO recorded at an excitation laser wavelength of 514.5 nm. (B) Raman image plotted with respect to the intensity of the G band. C1s XPS spectra of GO and rGO sheets: (C) GO sheets and (D) GO reduced with hydrazine vapor.

and oxygen were summarized to show the quantitative defects in GO and rGO materials (Table 2). After GO was treated with hydrazine, the carbon ratio increases from 57.7 to 73.6, but the oxygen ratio decreased from 42.3 to 26.4, indicating that the reactive oxygen-containing functionalities in GO were significantly decreased by hydrazine.[43,44] Similar to the vertical alignment of H_2Pc nanofibers on Ag surfaces, weakly interacting rGO surfaces can be obtained upon increasing the value of T_{sub}, as a result of decreasing the surface energy;[31] accordingly, weak molecule–substrate interactions allow relatively high degrees of molecular desorption and diffusion, ultimately causing molecule–molecule (*i.e.*, π–π and van der Waals) interactions to become dominant contributors to the H_2Pc nanofiber formation.[45] Because molecular stacking occurs mainly through molecule–molecule interactions when nonpolar molecules (*e.g.*, perylene,[46] coronene,[47] and MPcs[25,26]) form 1D nanofibers, we suspect that both face-to-face (π stacking) and edge-to-edge (van der Waals interactions) intermolecular forces are major contributors during the 1D self-assembly of the stacking planar H_2Pc molecules.[45] By balancing these crucial properties, we also explored the ability of various small organic molecules (CuPc, coronene and DAAQ) to aggregate into well-aligned 1D nanostructures on rGO surfaces (see Fig. S1†). Therefore, this practical rGO coating appears to effectively induce the out-of-plane morphological growth of small organic molecules for use as organic active layers in most optoelectronic devices. From prior reports of organic electronics applications,[25,26] MPc molecules prefer to form 1D out-of-plane nanostructures on noble metal (*e.g.*, Au, Ag) surfaces upon adjusting the value of T_{sub}. Therefore, we selected the Ag/ITO substrate as a reference to further understand the correlation between the morphologies and FE characteristics of the H_2Pc nanofiber films formed on the rGO/ITO surfaces.

From the point of view of FE applications, the field enhancement factor (β) is approximated by the aspect ratio (AR; length-to-radius ratio) of a 1D nanostructure:

$$AR = (\text{mean length; } L)/(\text{mean radius; } r_m).$$

The dimensions of a 1D nanostructure having a higher AR would provide a larger geometrical field enhancement and a lower turn-on field.[48] Here, we changed the deposition time to optimize the length of the nanofibers to improve the FE performance. The histograms of nanofiber lengths and radii of H_2Pc nanofiber films, deposited on the rGO/ITO and Ag/ITO substrates, were determined for subsequent FE applications [Fig. 4(A, C) and (B, D), respectively]. The values of L and r_m of the H_2Pc nanofibers deposited on the rGO/ITO substrate were 1175 ± 440 and 42.0 ± 13.2 nm, respectively (AR = 28); H_2Pc nanofiber films fabricated on the Ag substrate had smaller

Table 2 Atomic percentages of carbon and oxygen (from XPS data, calculated using the Shirley method)

Films	At.% of Carbon	At.% of Oxygen
GO	57.7	42.3
rGO	73.6	26.4

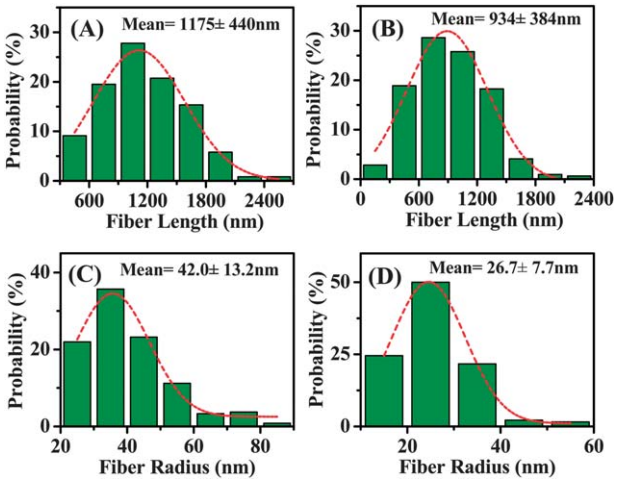

Fig. 4 (A–D) Histograms of the fiber length and fiber radius of the H_2Pc nanofibers deposited on (A, C) rGO and (B, D) Ag surfaces at a value of T_{sub} of 230 °C.

dimensions (934 ± 384 and 26.7 ± 7.7 nm, respectively; AR = 35). Fig. 5(A) and (C) display the TEM images of H_2Pc nanofibers synthesized on the rGO/ITO and Ag/ITO substrates; no catalyst is evident at the tips after applying this fabrication process. The HRTEM images of a single H_2Pc nanofiber [Fig. 5(B) and (D), respectively] both feature indistinct lattice fringe spacing, suggesting that the H_2Pc molecules were stacked in short-range order and entangled randomly within the nanofiber. The corresponding SAED patterns of an individual H_2Pc nanofiber indicate that the H_2Pc nanofibers formed on the rGO/ITO and Ag/ITO substrates were both polycrystalline [Fig. 5(B) and (D), insets].

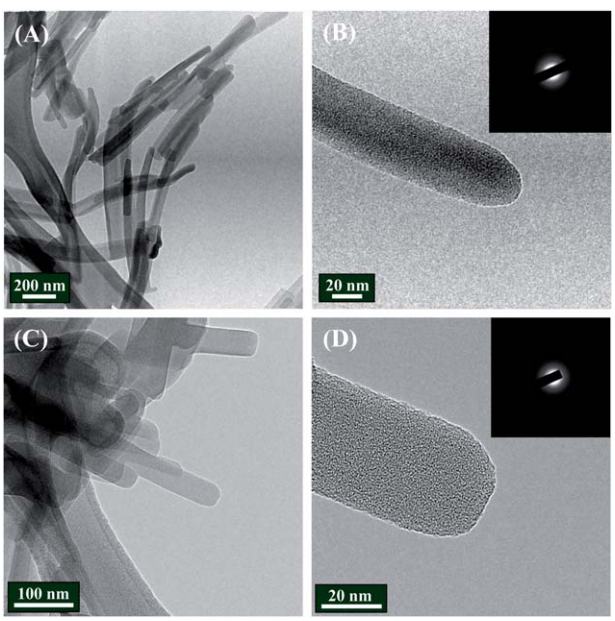

Fig. 5 TEM images of H_2Pc nanofibers formed on the (A) rGO/ITO and (C) Ag/ITO substrates. HRTEM images of a single nanofiber formed on the (B) rGO/ITO and (D) Ag/ITO substrates; insets: corresponding SAED patterns.

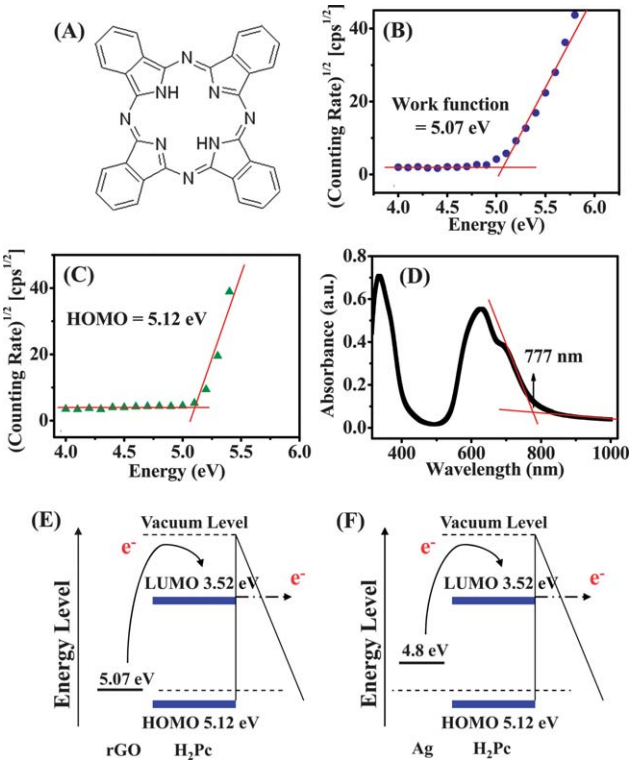

Fig. 6 (A) Molecular structure of H_2Pc. (B) The rGO work function, measured using PESA. (C) PESA analysis and (D) UV–Vis absorption spectrum of the H_2Pc thin film. (E, F) Schematic representations of the energy levels and electrons field emitted through the H_2Pc nanofibers of the (E) rGO-H_2Pc and (F) Ag-H_2Pc contacts.

Fig. 6(A) presents the molecular structure of H_2Pc. To further determine the energy levels of the rGO and H_2Pc materials for potential FE applications, we used PESA to measure the work function of the rGO films and the HOMO energy level of the H_2Pc materials [Fig. 6(B, C)] and UV–Vis spectroscopy [Fig. 6(D)] to measure the energy gap. Using the supplied software, we fitted the PESA data through linear extrapolation of the value of $CPS^{1/2}$ to zero yields, obtaining a work function for rGO films of 5.07 eV and a HOMO energy level for the H_2Pc films of 5.12 eV relative to the vacuum level. The UV–Vis spectrum of the H_2Pc film, in the region 300–1000 nm, revealed overlapping of the two main bands with maxima at 630 and 700 nm. From the onset wavelength at 777 nm, we derived the energy gap for the H_2Pc materials of 1.60 eV, thereby obtaining a lowest unoccupied molecular orbital (LUMO) energy level of 3.52 eV. Schematic representations of the energy levels revealed that the active layer of H_2Pc materials was suitable for FE on both the rGO and Ag electrodes [Fig. 6(E, F)]. The FE devices of the H_2Pc nanofiber films prepared on the rGO substrate are denoted herein as "**FE-rGO**", while the FE devices of those prepared on the Ag/ITO substrate are denoted as "**FE-Ag**". Comparing the schematic energy level diagrams of both FE devices, we obtained work functions of the cathode substrates (rGO and Ag) of 5.07 and 4.8 eV, respectively, suggesting that the electron injection barrier of the **FE-Ag** device was slightly smaller than that of the **FE-rGO** device.

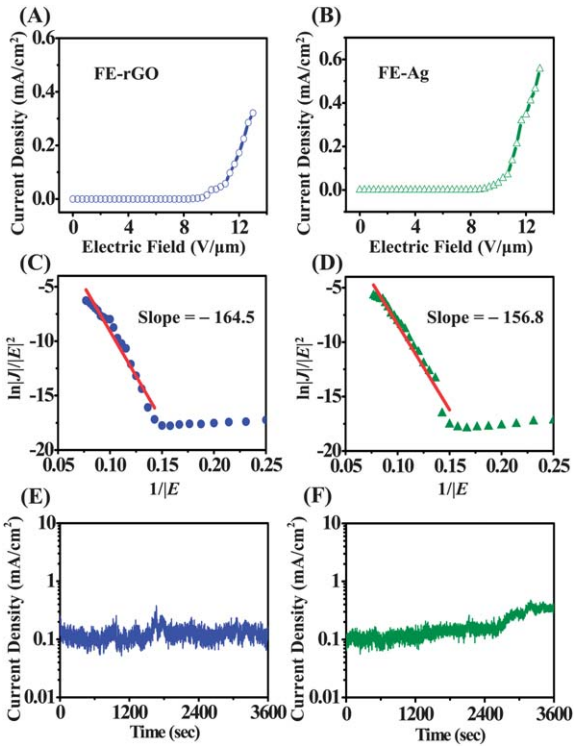

Fig. 7 Field emission J–E curves and corresponding FN plots of (A, C) **FE-rGO** and (B, D) **FE-Ag**. Emission current stability plots of (E) **FE-rGO** and (F) **FE-Ag** recorded for 3600 s under a constant applied field.

Fig. 7(A, B) display typical plots of the emission current (J) with respect to the applied field (E) for the **FE-rGO** and **FE-Ag** devices. The turn-on fields (defined as the applied field required for a current density of 10 μA cm^{-2}) of the **FE-rGO** and **FE-Ag** devices were 9.7 and 9.3 V μm^{-1}, respectively; at an applied field of 13 V μm^{-1}, the maximum current densities were 0.32 and 0.56 mA cm^{-2}, respectively. These FE properties of **FE-rGO** have great potential as a competitive candidate for field emitters.[49–51] The Fowler–Nordheim (FN) equation describes the dependence of the emission current of a field emitter on the applied field.[52] By plotting $\ln(J/E^2)$ with respect to $1/E$, the slope of the line of best fit can be used to deduce the field enhancement factor (β):

$$\beta = -\frac{6.83 \times 10^3 \phi^{3/2}}{S} \quad (3)$$

where S is the slope of the FN plot and ϕ is the local work function of the emitter material. Normally, β is inversely proportional to the tip's radius, as a result of its electrostatic properties.[48] The larger radius of the nanofibers in **FE-rGO**, relative to those in **FE-Ag**, resulted in a lower value of β and a higher turn-on electric field. The linear FN plots in Fig. 7(C, D) reveal that the J–E characteristics of the H_2Pc nanofibers followed the FN field emission mechanism, indicating that the electron transport from the H_2Pc nanomaterials to the vacuum level was a quantum tunneling process in an applied field.[25,26] The slopes of the FN plots (S) for the **FE-rGO** and **FE-Ag** devices were −164.5 and −156.8, respectively. By taking 3.52 eV as the LUMO energy level (ϕ) for H_2Pc materials, obtained from the PESA and UV–Vis measurements, we estimated the values of β of these two field emitters to be 274 and 288, respectively.

Next, we performed stability measurements of the **FE-rGO** and **FE-Ag** emitters for 3600 s under an applied field of 12 V μm^{-1}; Fig. 7(E, F) present the plots of the FE current density (J) with respect to the testing time. The calculated mean current densities for **FE-rGO** and **FE-Ag** were approximately 0.12 and 0.17 mA cm^{-2}, respectively. Both emitters exhibited stable emission properties, merely featuring a slow increase in the emission current over time, which might correspond to a training effect involving the removal of impurities from the H_2Pc nanofibers.[30] Relative to **FE-Ag**, the **FE-rGO** devices not only exhibited more-stable FE properties but might also have greater utility because of the potential for large-scale production of rGO. From our optical and electrical analyses of the rGO-based FE devices, it appears that rGO is a unique coating material for minimizing the surface energy of electrodes and has better optical transmittance than that of conventional noble metal films (*e.g.*, Au, Ag). Our graphene-assisted synthesis of 1D small-organic-molecule nanostructures is a feasible process that opens a new avenue for manipulating the morphologies of active layers used in organic electronics (*e.g.*, field emitters, sensors, photovoltaics).

4. Conclusions

Temperature control of rGO-coated electrodes can assist H_2Pc molecules to form out-of-plane nanofiber structures when using a conventional TE process. Devices presenting well-aligned 1D H_2Pc nanofiber films on rGO/ITO exhibited excellent FE characteristics and followed FN behavior. Comparing FE devices containing the rGO/ITO and Ag/ITO as electrodes, we found that the emission currents were 0.32 mA cm^{-2} for **FE-rGO** and 0.56 mA cm^{-2} for **FE-Ag** (when biased at an applied field of 13 V μm^{-1}), with turn-on electric fields of 9.7 and 9.3 V μm^{-1}, respectively. From the slopes of FN plots, we estimated the values of β of these emitters to be 274 and 288, respectively. From FE stability tests, the current densities of **FE-rGO** devices underwent fluctuations of less than 30%, revealing stable and excellent performances within the testing duration. Because of the outstanding optical and electrical properties of graphene-coated ITO electrodes, we believe that this facile platform for rGO coating will be competitive with that of noble metal electrodes for inducing the growth of nanofiber structures of small organic molecules on targeting surfaces. This firsthand attempt at using solution processing of rGO coatings to fabricate H_2Pc nanofiber FE devices opens up the potentially interesting research field of the synthesis of 1D nanofibers as active layers on transparent electrodes, without the corresponding poor optical transmission found with traditional metal coatings.

Acknowledgements

We thank the National Science Council of Taiwan, ROC, for financial support (project NSC 100-2221-E-009-023-MY3).

References

1 A. K. Geim and K. S. Novoselov, *Nat. Mater.*, 2007, **6**, 183.
2 A. K. Geim, *Science*, 2009, **324**, 1530.
3 G. Eda, G. Fanchini and M. Chhowalla, *Nat. Nanotechnol.*, 2008, **3**, 270.
4 C. Gómez-Navarro, M. Burghard and K. Kern, *Nano Lett.*, 2008, **8**, 2045.
5 X. Wang, L. Zhi and K. Müllen, *Nano Lett.*, 2008, **8**, 323.
6 A. A. Balandin, S. Ghosh, W. Bao, I. Calizo, D. Teweldebrhan, F. Miao and C. N. Lau, *Nano Lett.*, 2008, **8**, 902.
7 P. Blake, P. D. Brimicombe, R. R. Nair, T. J. Booth, D. Jiang, F. Schedin, L. A. Ponomarenko, S. V. Morozov, H. F. Gleeson, E. W. Hill, A. K. Geim and K. S. Novoselov, *Nano Lett.*, 2008, **8**, 1704.
8 K. S. Kim, Y. Zhao, H. Jang, S. Y. Lee, J. M. Kim, K. S. Kim, J. H. Ahn, P. Kim, J. Y. Choi and B. H. Hong, *Nature*, 2009, **457**, 706.
9 D. Li, M. B. Müller, S. Gilje, R. B. Kaner and G. G. Wallace, *Nat. Nanotechnol.*, 2008, **3**, 101.
10 S. Park and R. S. Ruoff, *Nat. Nanotechnol.*, 2009, **4**, 217.
11 W. S. Hummers and R. E. Offeman, *J. Am. Chem. Soc.*, 1958, **80**, 1339.
12 X. Liang, Z. Fu and S. Y. Chou, *Nano Lett.*, 2007, **7**, 3840.
13 M. J. Allen, V. C. Tung, L. Gomez, Z. Xu, L. M. Chen, K. S. Nelson, C. Zhou, R. B. Kaner and Y. Yang, *Adv. Mater.*, 2009, **21**, 2098.
14 V. Dua, S. P. Surwade, S. Ammu, S. R. Agnihotra, S. Jain, K. E. Roberts, S. Park, R. S. Ruoff and S. K. Manohar, *Angew. Chem., Int. Ed.*, 2010, **49**, 2154.
15 K. Y. Shin, J. Y. Hong and J. Jang, *Adv. Mater.*, 2011, **23**, 2113.
16 J. Blochwitz, M. Pfeiffer, T. Fritz and K. Leo, *Appl. Phys. Lett.*, 1998, **73**, 729.
17 J. Zhang, H. Wang, X. Yan, J. Wang, J. Shi and D. Yan, *Adv. Mater.*, 2005, **17**, 1191.
18 R. W. I. de Boer, A. F. Stassen, M. F. Craciun, C. L. Mulder, A. Molinari, S. Rogge and A. F. Morpurgo, *Appl. Phys. Lett.*, 2005, **86**, 262109.
19 J. Wang, H. Wang, X. Yan, H. Huang and D. Yan, *Appl. Phys. Lett.*, 2005, **87**, 093507.
20 Q. Tang, H. Li, M. He, W. Hu, C. Liu, K. Chen, C. Wang, Y. Liu and D. Zhu, *Adv. Mater.*, 2006, **18**, 65.
21 F. Yang, M. Shtein and S. R. Forrest, *J. Appl. Phys.*, 2005, **98**, 014906.
22 F. Yang, M. Shtein and S. R. Forrest, *Nat. Mater.*, 2005, **4**, 37.
23 Y. S. Hsiao, W. T. Whang, S. C. Suen, J. Y. Shiu and C. P. Chen, *Nanotechnology*, 2008, **19**, 415603.
24 W. Y. Tong, Z. X. Li, A. B. Djurišić, W. K. Chan and S. F. Yu, *Mater. Lett.*, 2007, **61**, 3842.
25 S. C. Suen, W. T. Whang, F. J. Hou and B. T. Dai, *Org. Electron.*, 2006, **7**, 428.
26 K. J. Huang, Y. S. Hsiao and W. T. Whang, *Org. Electron.*, 2011, **12**, 1826.
27 J. A. Venables, G. D. T. Spiller and M. Hanbücken, *Rep. Prog. Phys.*, 1984, **47**, 399.
28 Y. S. Zhao, P. Zhan, J. Kim, K. Sun and J. Huang, *ACS Nano*, 2010, **4**, 1630.
29 A. B. Djurišić, A. M. C. Ng, K. Y. Cheung, M. K. Fung and W. K. Chan, *J. Mater. Sci. Technol.*, 2008, **24**, 563.
30 K. J. Huang, Y. S. Hsiao and W. T. Whang, *Org. Electron.*, 2011, **12**, 686.
31 A. W. Adamson, *Physical Chemistry of Surfaces*, John Wiley & Sons Publishers, 5th ed., 1990, p. 55.
32 D. K. Owens and R. C. Wendt, *J. Appl. Polym. Sci.*, 1969, **13**, 1741.
33 T. Sakurai, Y. Momose and K. Nakayama, *e-J. Surf. Sci. Nanotechnol.*, 2005, **3**, 179.
34 H. Peisert, M. Knupfer, T. Schwiege and J. Fink, *Appl. Phys. Lett.*, 2002, **80**, 2916.
35 H. He, T. Riedl, A. Lerf and J. Klinowski, *J. Phys. Chem.*, 1996, **100**, 19954.
36 H. He, J. Klinowski, M. Forster and A. Lerf, *Chem. Phys. Lett.*, 1998, **287**, 53.
37 Y. Xu, Z. Liu, Z. Zhang, Y. Wang, J. Tian, Y. Huang, Y. Ma, X. Zhang and Y. Chen, *Adv. Mater.*, 2009, **21**, 1275.
38 H. L. Wang, J. T. Robinson, X. L. Li and H. J. Dai, *J. Am. Chem. Soc.*, 2009, **131**, 9910.
39 A. B. Bourlinos, D. Gournis, D. Petridis, T. Szabó, A. Szeri and I. Dékány, *Langmuir*, 2003, **19**, 6050.
40 W. F. Zhao, M. Fang, F. R. Wu, H. Wu, L. W. Wang and G. H. Chen, *J. Mater. Chem.*, 2010, **20**, 5817.
41 M. S. Dresselhaus, G. Dresselhaus, R. Saito and A. Jorio, *Phys. Rep.*, 2005, **409**, 47.
42 S. Stankovich, D. A. Dikin, R. D. Piner, K. A. Kohlhaas, A. Kleinhammes, Y. Y. Jia, Y. Wu, S. T. Nguyen and R. S. Ruoff, *Carbon*, 2007, **45**, 1558.

43 K. S. Choi, Y. Park, K. C. Kwon, J. Kim, C. K. Kim, S. Y. Kim, K. Hong and J. L. Lee, *J. Electrochem. Soc.*, 2011, **158**, J231.
44 P. G. Ren, D. X. Yan, X. Ji, T. Chen and Z. M. Li, *Nanotechnology*, 2011, **22**, 055705.
45 H. Liu, J. Xu, Y. Li and Y. Li, *Acc. Chem. Res.*, 2010, **43**, 1496.
46 H. Liu, Y. Li, S. Xiao, H. Gan, T. Jiu, H. Li, L. Jiang, D. Zhu, D. Yu, B. Xiang and Y. Chen, *J. Am. Chem. Soc.*, 2003, **125**, 10794.
47 S. C. Suen, W. T. Whang, B. W. Wu and Y. F. Lai, *Appl. Phys. Lett.*, 2004, **84**, 3157.
48 F. G. Tarntair, C. Y. Wen, L. C. Chen, J. J. Wu, K. H. Chen, P. F. Kuo, S. W. Chang, Y. F. Chen, W. K. Hong and H. C. Cheng, *Appl. Phys. Lett.*, 2000, **76**, 2630.
49 H. Gan, H. Liu, Y. Li, Q. Zhao, Y. Li, S. Wang, T. Jiu, N. Wang, X. He, D. Yu and D. Zhu, *J. Am. Chem. Soc.*, 2005, **127**, 12452.
50 H. Liu, Q. Zhao, Y. Li, Y. Liu, F. Lu, J. Zhuang, S. Wang, L. Jiang, D. Zhu, D. Yu and L. Chi, *J. Am. Chem. Soc.*, 2005, **127**, 1120.
51 S. Cui, Y. Li, Y. Guo, H. Liu, Y. Song, J. Xu, J. Lv, M. Zhu and D. Zhu, *Adv. Mater.*, 2008, **20**, 309.
52 R. Fowler and L. W. Nordheim, *Proc. R. Soc. London, Ser. A*, 1928, **119**, 173.

